Supporting Information accompanying

STRUCTURAL BASIS FOR POTENCY AND PROMISCUITY IN POLY(ADP-RIBOSE) POLYMERASE (PARP) AND TANKYRASE INHIBITORS

Ann-Gerd Thorsell[a], Torun Ekblad[a], Tobias Karlberg[a], Mirjam Löw[a], Ana Filipa Pinto[a], Lionel Trésaugues[a], Martin Moche[b], Michael S. Cohen[c] and Herwig Schüler[a]

[a]Department of Medical Biochemistry and Biophysics and [b]Protein Science Facility/SciLifeLab, Karolinska Institutet, 17177 Stockholm, Sweden. [c]Program in Chemical Biology and Department of Physiology and Pharmacology, Health & Science University, Portland, Oregon 97210, USA.

Table of Contents

Supplemental Results

1. Proteins used in this study

The selection of protein constructs used in the enzymatic analysis is given in **Table S1**. PARP9 and -13 were excluded owing to their lack of ADP-ribosyltransferase activity;[1, 2] PARP6-8 and PARP11 could not be purified in amounts sufficient for biochemical characterization.

Table S1. Protein constructs used within this study*

Protein	Domain(s)**	Residues	Subclass***
PARP1/ARTD1	full length protein	M1-W1014	poly
PARP1/ARTD1	ZnF3-BRCT-WGR-ART	S224-W1014	poly
PARP1/ARTD1	ART	K662-T1011	poly
PARP2/ARTD2	full length protein	M1 –W583	poly
PARP2/ARTD2	ART	K176-W5383	poly
PARP3/ARTD3	full length protein	M1-H532	mono/poly
PARP3/ARTD3	ART	K178-H532	mono/poly
PARP4/ARTD4	ART	L250-S565	mono/poly
TNKS1/ARTD5	ART	Q1091-Q1325	poly
TNKS1/ARTD5	SAM-ART	T1017-Q1325	poly
TNKS2/ARTD6	ART	G952-G1166	poly
PARP10/ARTD10	full length protein	A809-G1017	mono
PARP12/ARTD12	ART	D489-S684	mono
PARP14/ARTD8	ART	D1611-1801	mono
PARP15/ARTD7	ART	N459-A656	mono
PARP16/ARTD15	ART	M1-K274	mono

*Alternative protein names are given in the first column. All proteins were produced in *Escherichia coli* from human cDNAs. **Domain designations: ART, ADP-ribosyltransferase domain, the "catalytic domain fragment" (including a regulatory subdomain in the cases of PARP1-4/ARTD1-4); BRCT, BRCA1 carboxy terminal homology; SAM, sterile alpha motif domain; WGR, WGR-motif containing nucleic acid binding domain; ZnF3, 3rd zinc finger domain. *** Poly, enzymes catalyzing the formation of poly-ADP-ribose chains on their substrates; mono, known or putative mono-ADP-ribosyltransferases. PARP3 and -4 likely catalyze mono-ADP-ribosylation preferentially[2] but share the subdomain arrangement of the catalytic fragment with PARP1 and -2.

2. Enzymatic assay validation

An assay for PARP activity based on detection of incorporated biotin-ADP-ribose derived from a low percentage of biotin-NAD^+ in the reaction has been described earlier,[3, 4, 5] and is used in several commercial kits. Here, we used the same principle. For an independent validation of this assay, we first determined the linear range of signals obtained by a dilution series of biotin-ADP-ribosylated enzyme (**Fig. S1A**). The result shows that the signal is linear

over a wide range of biotin-ADP-ribosyl concentrations. All measurements in this study were conducted within this linear signal range. Next, we performed control experiments to verify that the biotin moiety had no effect on dinucleotide binding (**Fig. S1B**). The results indicate that, within experimental error and enzyme batch-to-batch variation, the biotin moiety does not affect the kinetics of ADP-ribosylation in the range between 0.5 and 10 % biotin-NAD$^+$. In all other experiments, the content of biotin-NAD$^+$ used was 2 % of total NAD$^+$.

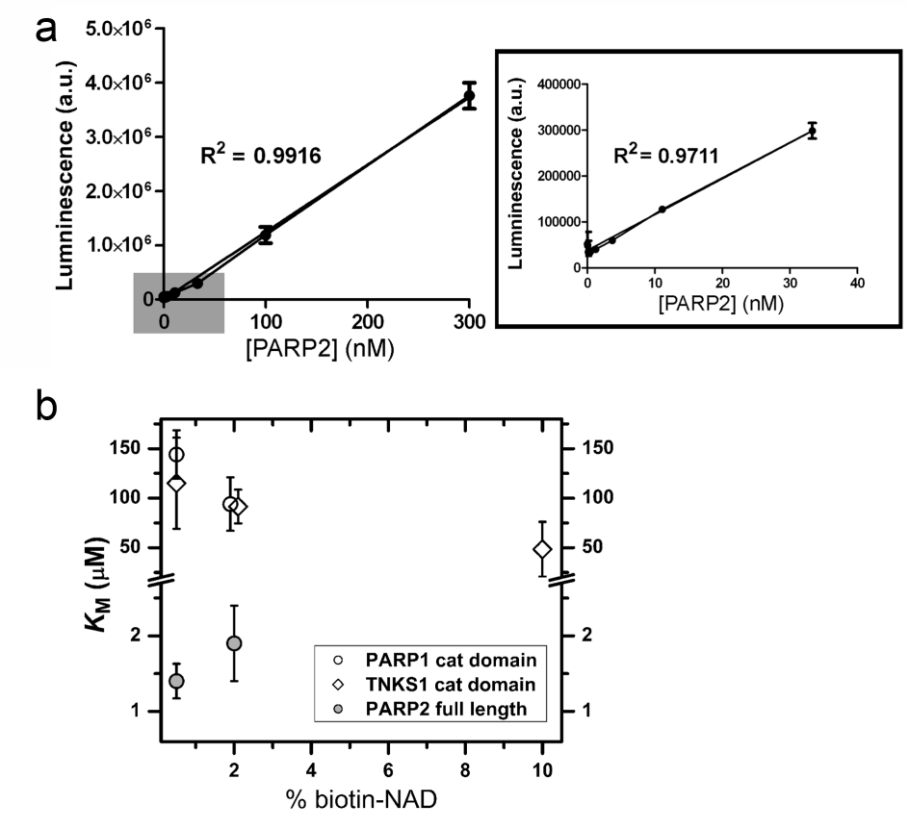

Figure S1. Validation of a general ADP-ribosyltransferase assay. (A) Linear range of the luminescence signal. Full length PARP2 protein (3 µM) was subjected to automodification in presence of 2% biotinylated NAD$^+$. A dilution series of the protein was then processed under typical assay conditions (see Methods section of main text). Inset: magnification of the area shaded gray in the main diagram. (B) The assay measures incorporation of biotin-NAD$^+$ into PARP target sites. To test whether biotin-NAD$^+$ was incorporated at similar rates as unlabeled NAD$^+$, reaction rates were determined at different [biotin-NAD$^+$] for three proteins and the resulting K_M values were plotted against the percentage of biotin-NAD$^+$. K_M values were within experimental error independent of [biotin-NAD$^+$] and we conclude that the biotin moiety does not interfere with cofactor binding.

3. K_M values for 11 PARP enzymes

We determined K_M^{NAD+} for eleven PARP family members (**Figure S2** and **Table S2**). Values vary from low micromolar (PARP1 and -2) to high micromolar (PARP16). Z'-factors determined based on data from these experiments indicate that the assay is well suited for enzyme inhibition studies. For full length PARP1 and -2, K_M values have been determined by others before; in both cases we determined are significantly lower values than the ones previously published (see main text, **Table 1**). We determined a 10-fold lower value for our in-house enzyme, purified using IMAC only, than for commercial full length PARP1.

Table S2. K_M^{NAD+} values for human PARP enzymes.*

Protein	Domain(s)	K_M (µM)	Z'-factor**
PARP1	full length protein	0.78±0.45	0.91
PARP1	commercial, full length	7.1±1.3	0.81
PARP1	ZnF3-BRCT-WGR-ART	247±42	0.92
PARP1	ART	94±27	0.96
PARP2	full length protein	1.9±0.5	0.91
PARP2	ART	84±6.2	0.96
PARP3	full length protein	131±57	0.92
PARP3	ART	2170±645	0.69
PARP4	ART	92±17	0.71
TNKS1	ART	30.9±4.0	0.97
TNKS1	SAM-ART	40.6±10.7	0.93
TNKS2	ART	251±56	0.95
PARP10	full length protein	98±11	0.87
PARP10	ART	90±27	0.98
PARP12	ART	299±76	0.99
PARP14	ART	62±7.0	0.99
PARP15	ART	11.0±4.2	0.94
PARP16	full length protein	582±196	0.61

*Experimental data are shown in Supplementary Figure 3. **Calculated at [NAD] ≤ K_M

The 3rd zinc finger domain of PARP1 mediates DNA-dependent PARP activity,[6, 7] whereas the 1st zinc finger domain is needed to obtain full PARP1 activity,[5] and Zn1 and Zn3 together may be sufficient for full activity of the catalytic fragment.[3] Here we measured the activity of PARP1 construct 224-1014, spanning the 3rd zinc finger domain up to the C-terminus. We found that this PARP1 construct has ~250-fold lower activity (in terms of K_M for DNA-stimulated automodification) than the full length protein, and is less active than the isolated catalytic domain fragment (**Figure S2**).

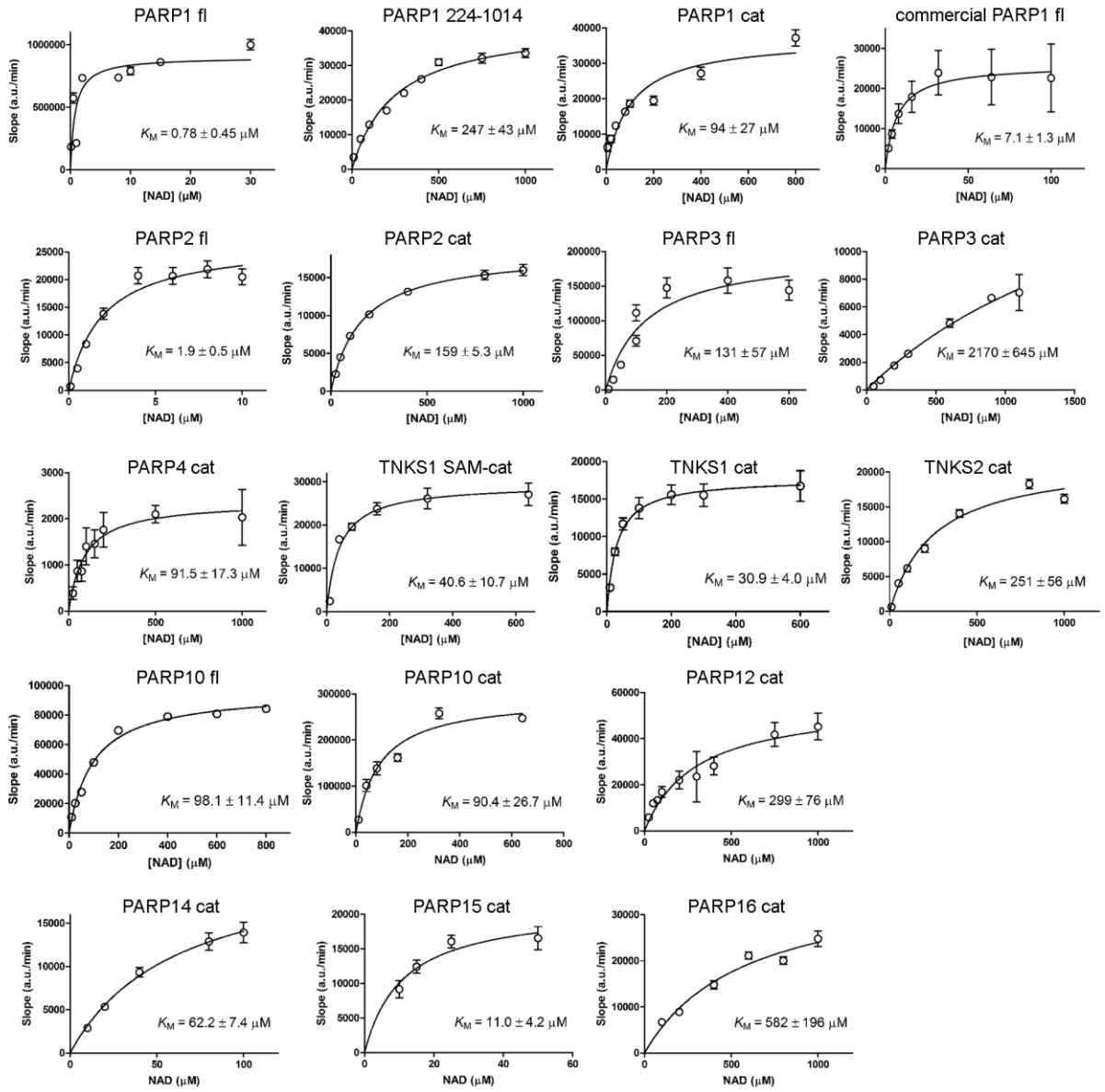

Figure S2. Determination of Michaelis-Menten kinetics of various PARP enzyme constructs. Non-linear regression plots of the NAD^+-dependent ADP-ribosylation rates (experimental data underlying the K_M^{NAD+} values reported in Figure 1b and Table 1 of the main text as well as Table S2 above). Protein construct domain contents are indicated (fl, full length proteins; cat, catalytic domain fragments).

4. Inhibition of 10 PARP family members by 7 PARP inhibitors

Results were generally reproducible between batches of compounds and proteins. PARP16 is an exception; here we systematically observed partial compound induced enzyme aggregation, and were unable to identify conditions under which we could reliably determine IC_{50} values. We also noted that PARP16 was significantly more prone to DMSO-induced inactivation than any other enzymes in this study. Thus we can only report results for PARP16 inhibition by three of the compounds. Compound induced aggregation was also observed with PARP12 and in these instances IC_{50} values are not reported. The final results of this study are summarized in **Table 2** and **Table 3** of the main text, and experimental data are shown in **Figs. S3 - S12**.

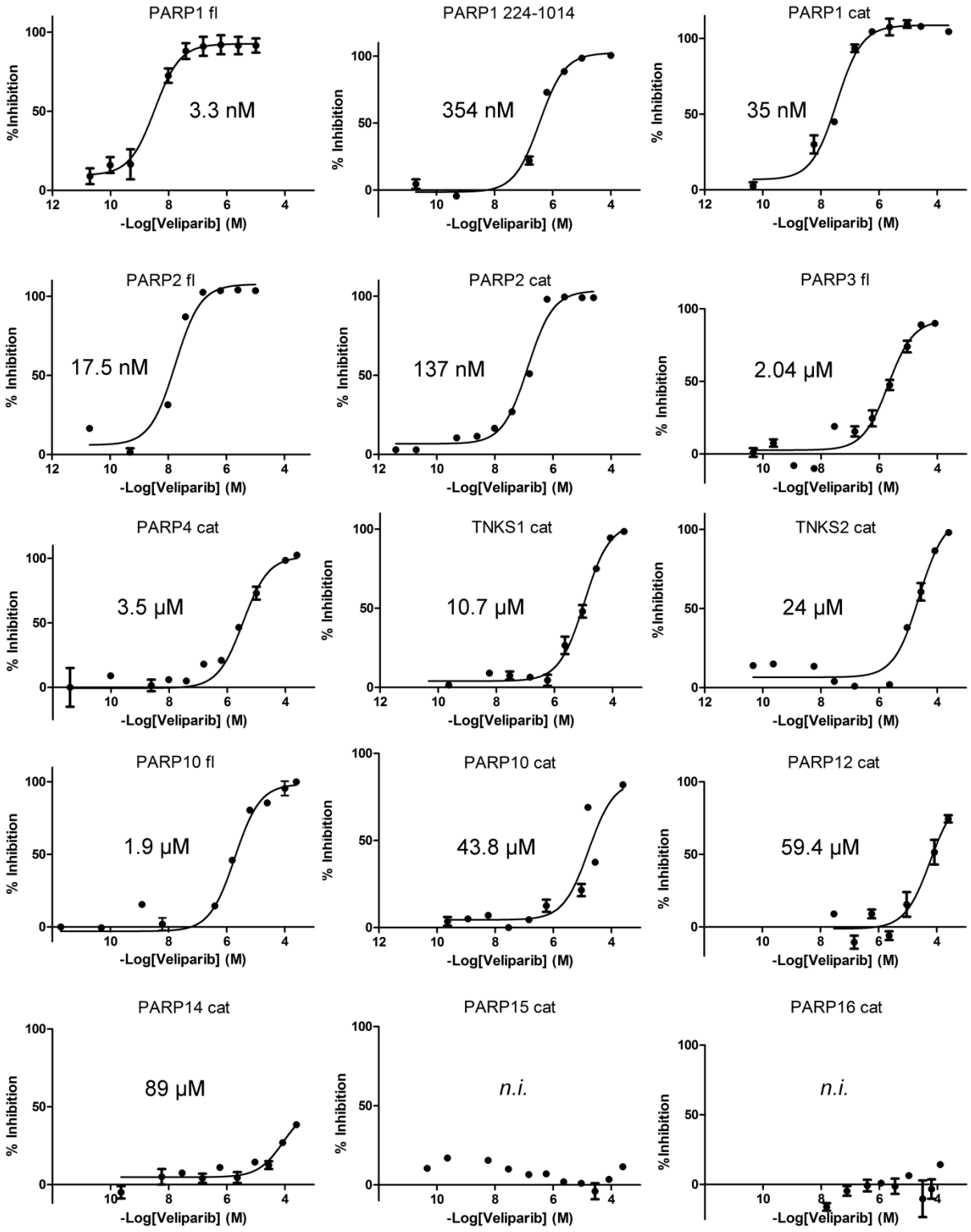

Figure S3. Concentration response curves for Veliparib-dependent inhibition of ADP-ribosyltransferases. The IC_{50} value calculated from each data set is indicated.

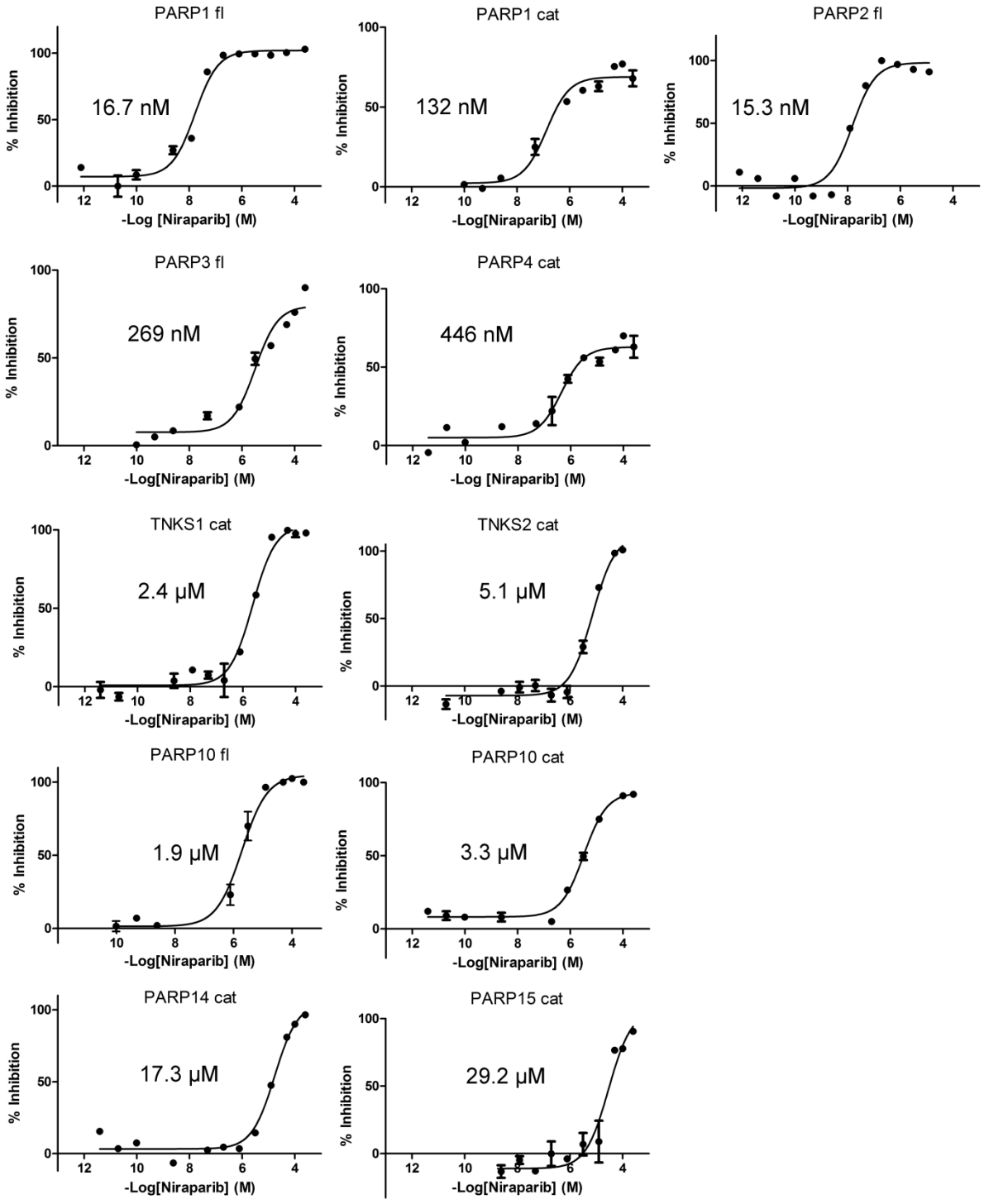

Figure S4. Concentration response curves for Niraparib-dependent inhibition of ADP-ribosyltransferases. The IC_{50} value calculated from each data set is indicated.

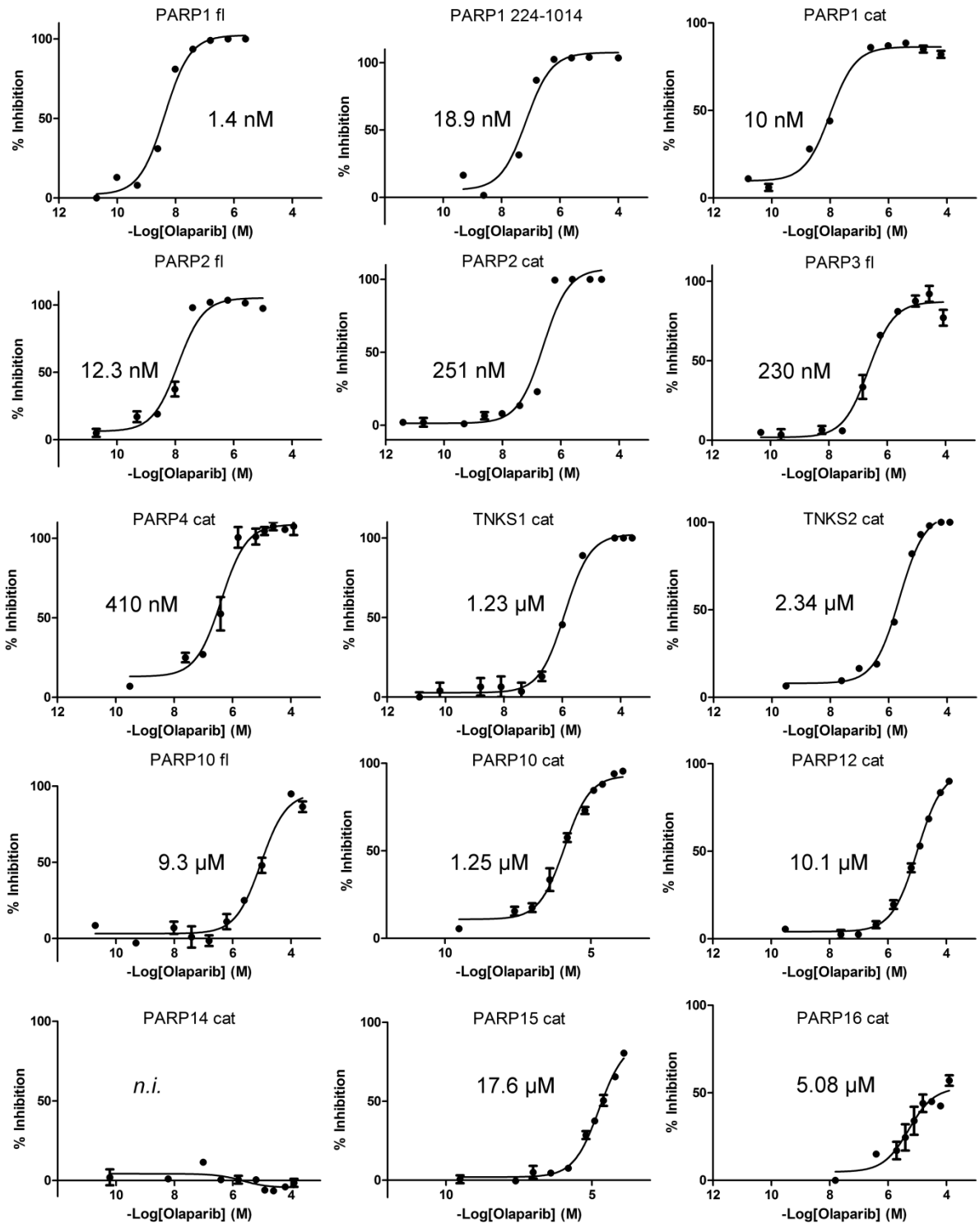

Figure S5. Concentration response curves for Olaparib-dependent inhibition of ADP-ribosyltransferases. The IC_{50} value calculated from each data set is indicated.

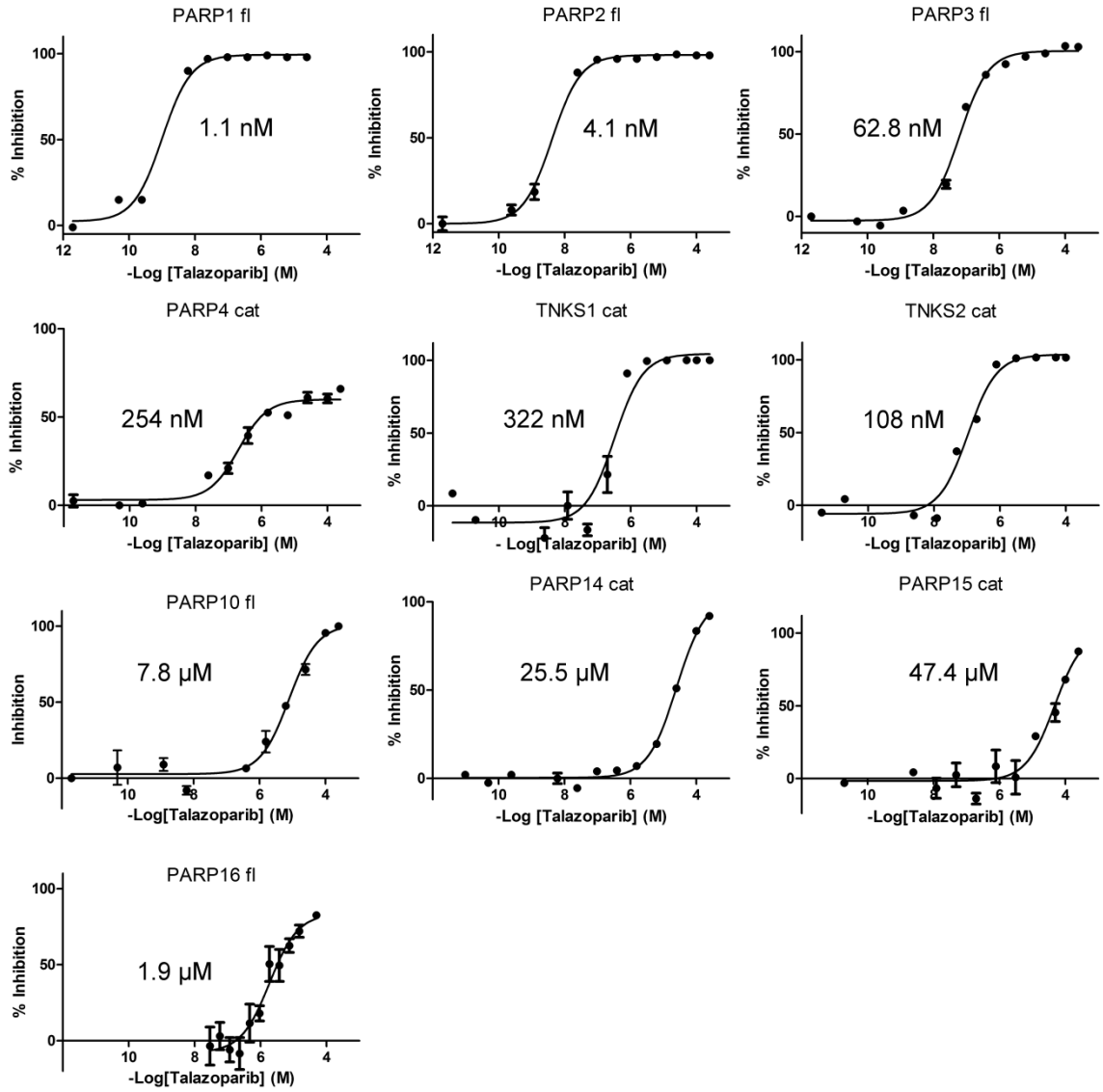

Figure S6. Concentration response curves for Talazoparib-dependent inhibition of ADP-ribosyltransferases. The IC_{50} value calculated from each data set is indicated.

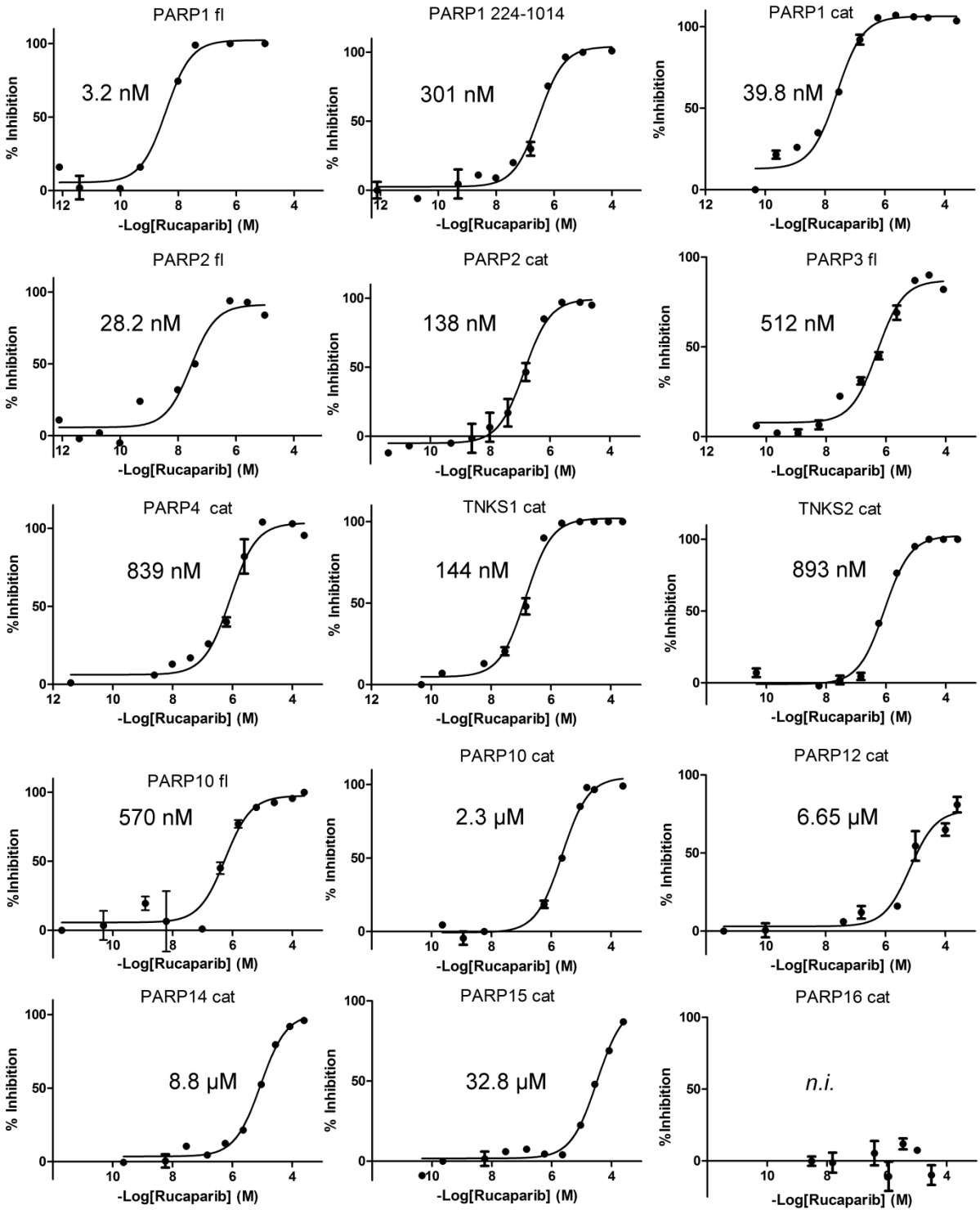

Figure S7. Concentration response curves for Rucaparib-dependent inhibition of ADP-ribosyltransferases. The IC_{50} value calculated from each data set is indicated.

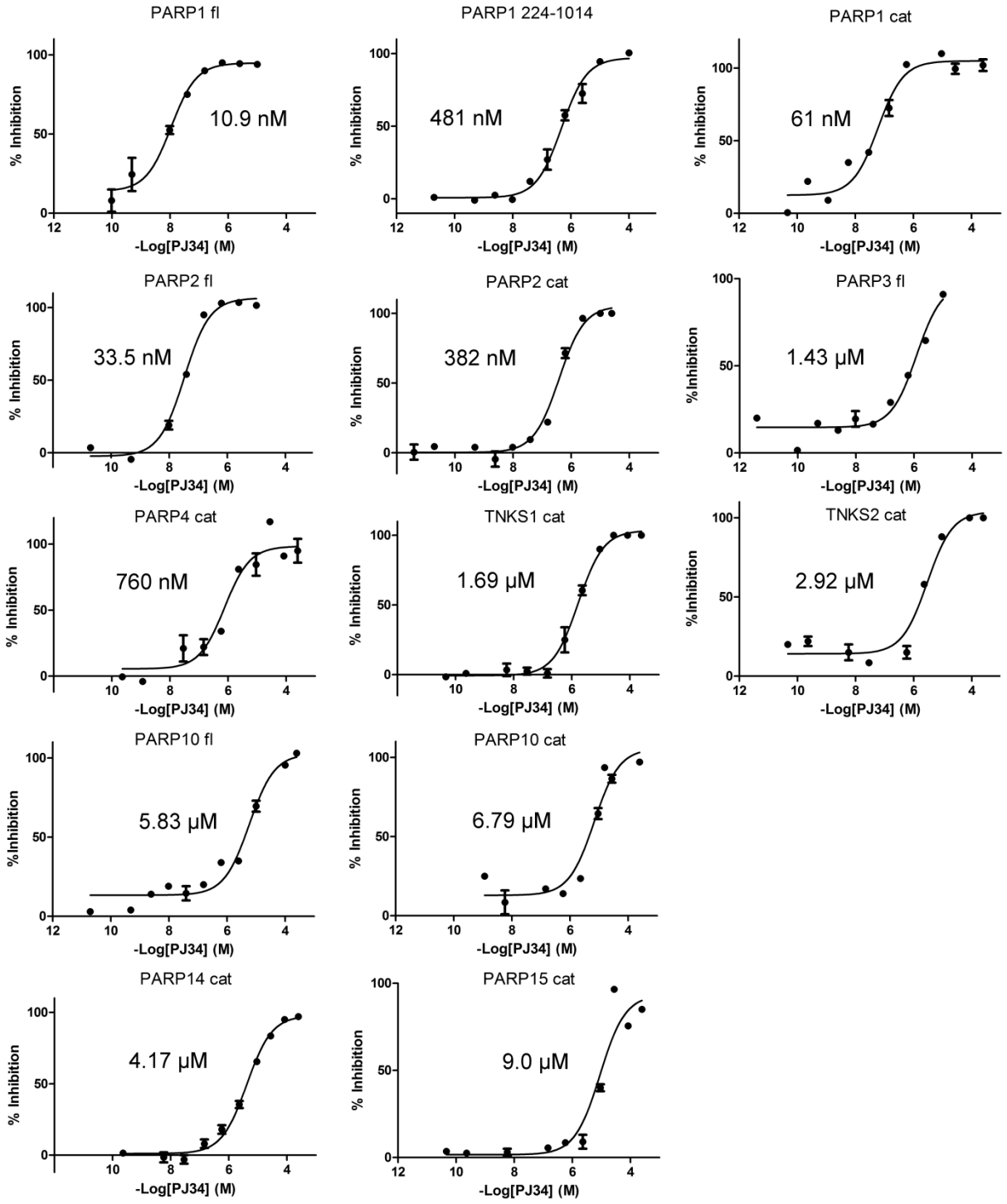

Figure S8. Concentration response curves for PJ34-dependent inhibition of ADP-ribosyltransferases. The IC_{50} value calculated from each data set is indicated.

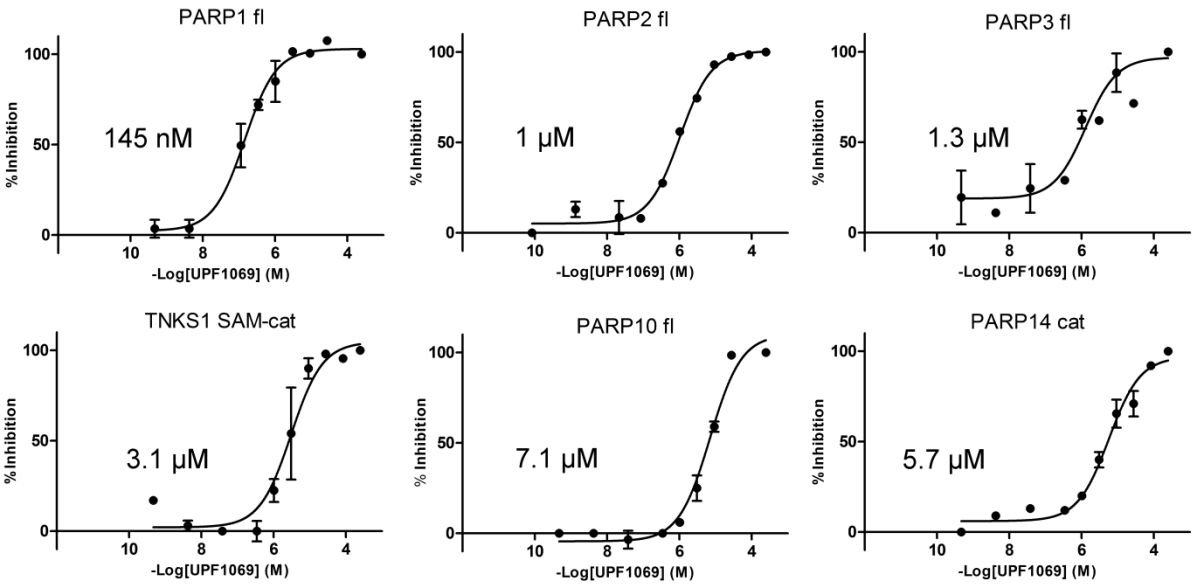

Figure S9. Concentration response curves for UPF1069-dependent inhibition of ADP-ribosyltransferases. The IC_{50} value calculated from each data set is indicated.

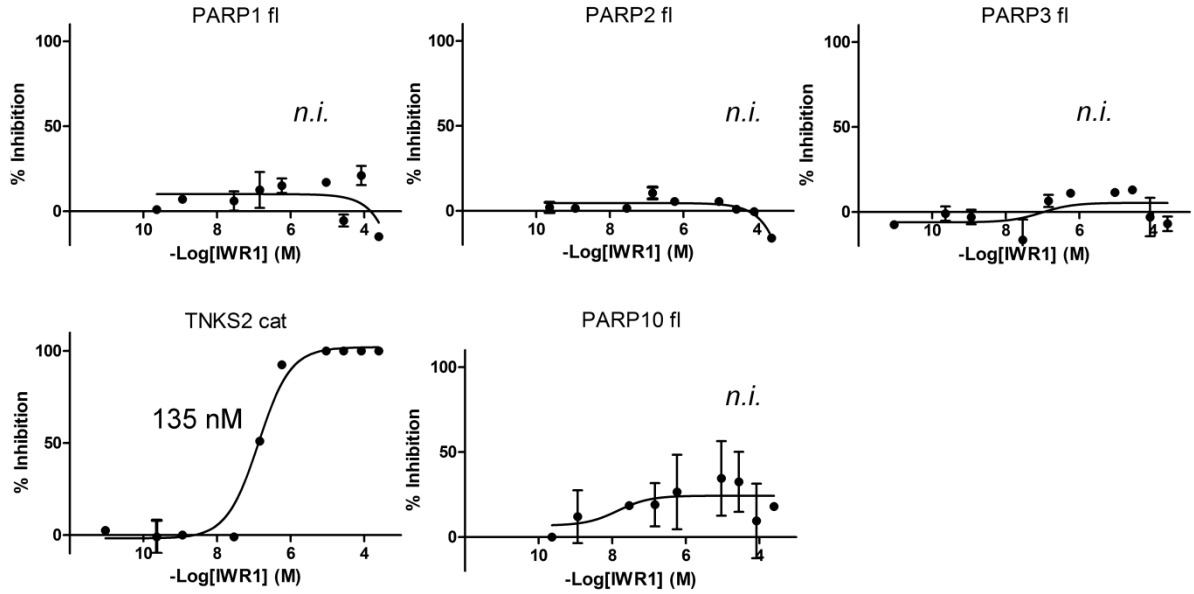

Figure S10. Concentration response curve for IWR1-dependent inhibition of tankyrase-2. The IC_{50} value calculated from this data set is indicated. Inhibition of tankyrase-1 was not measured; for the PARP1, -2, 3- and 10 full length enzymes no inhibition was observed.

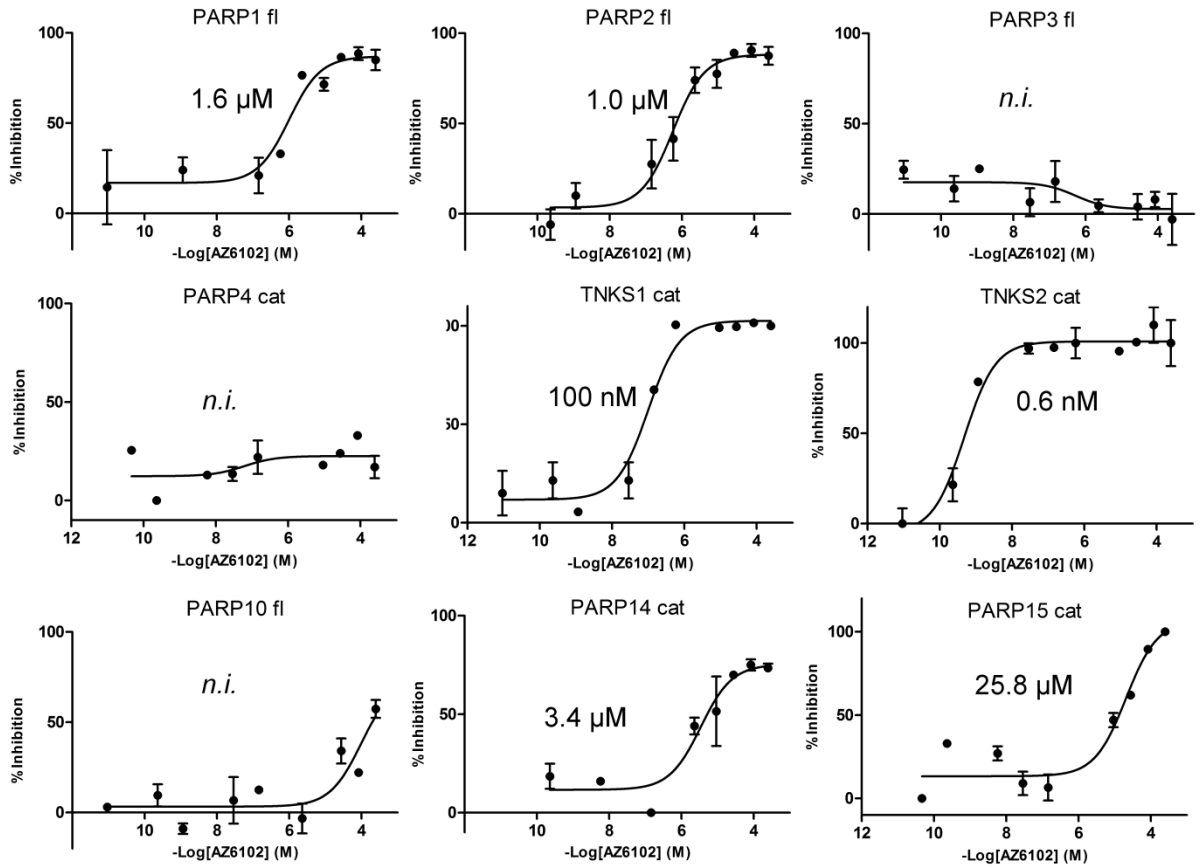

Figure S11. Concentration response curves for AZ6102-dependent inhibition of ADP-ribosyltransferases. The IC_{50} value calculated from each data set is indicated.

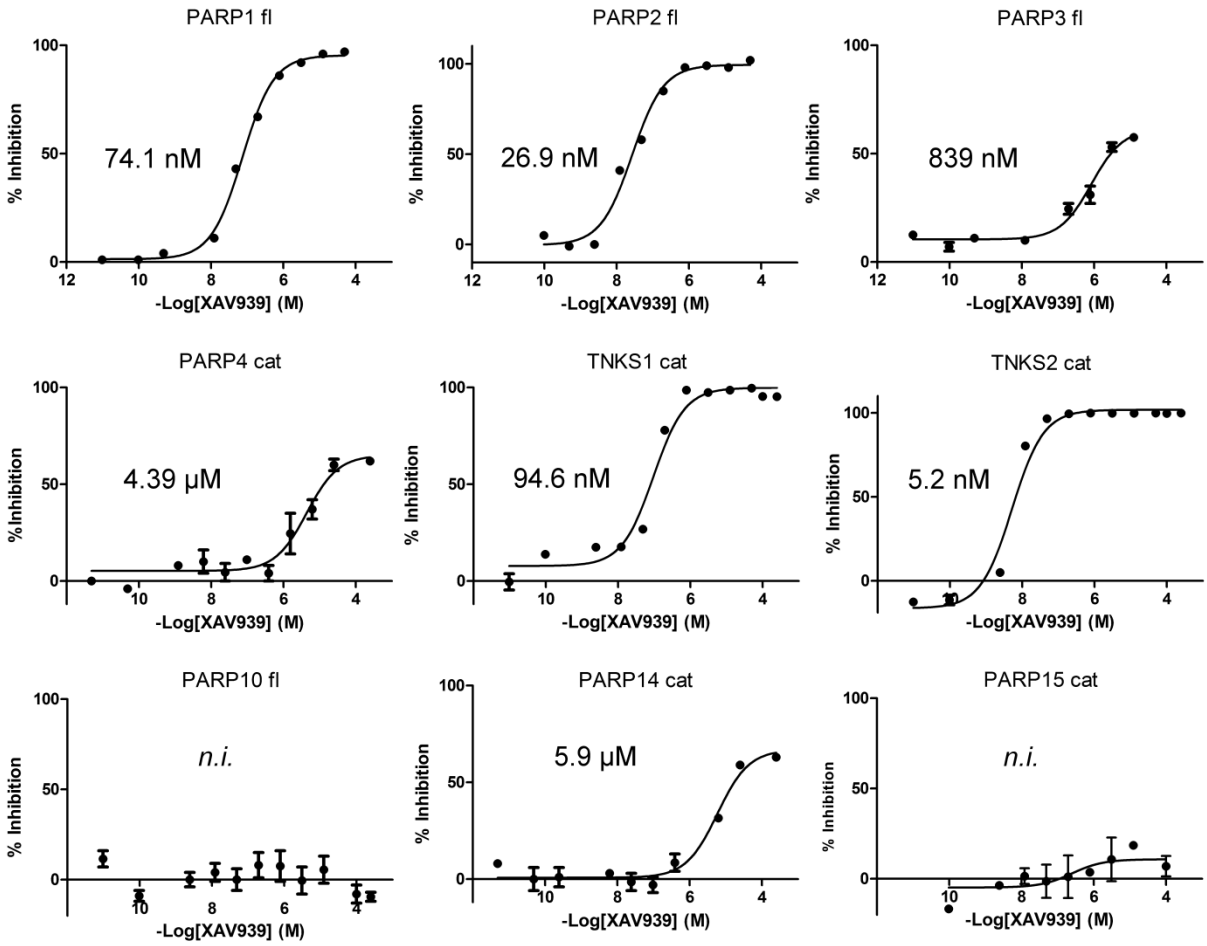

Figure S12. Concentration response curves for XAV939-dependent inhibition of ADP-ribosyltransferases. The IC_{50} value calculated from each data set is indicated.

Table S3. Crystallographic data collection and refinement statistics.

Protein	**PARP1**	**PARP2**	**PARP1**	**PARP1**	**PARP1**	**PARP1**	**PARP10**
Ligand	**Niraparib**	**Olaparib**	**Rucaparib**	**Talazoparib**	**PJ34**	**XAV939**	**Veliparib**
PDB entry	4R6E	4TVJ	4RV6	4UND	4UXB	4R5W	5LX6
Data collection							
Synchrotron	DIAMOND	DIAMOND	BESSY	BESSY	DIAMOND	BESSY	DIAMOND
Beam line	I03	I04	BL14.2	BL14.1	I24	BL14.2	I04
Wavelength (Å)	0.97630	0.99190	0.91841	0.91841	0.96865	0.91841	0.92819
Space group	$P2_12_12_1$	$P2_1$	P2	$P4_12_12$	F222	$P2_1$	$P2_1$
a, b, c (Å)	104.40, 108.64, 142.20	58.1, 134.1, 58.4	93.63, 85.10, 101.95	103.46, 103.46,168.5	105.24, 166.42, 182.95	74.52, 67.66, 91.17	52.48, 88.68, 52.40
α, β, γ (°)	90, 90, 90	90, 117.96, 90	90, 100.97, 90	90, 90, 90	90, 90, 90	90, 111.28, 90	90, 104.68, 90
Resolution (Å)[a]	86.3 - 2.20 (2.26 - 2.20)	30.0 – 2.10 (2.15 -2.10)	48.0 - 3.19 (3.38 - 3.19)	50.0 - 2.20 (2.28 - 2.20)	47.4 – 3.22 (3.39 - 3.22)	50.0 - 2.83 (3.01 - 2.83)	47.65-1.25 (1.32-1.25)
Unique reflections[a]	82734 (6064)	45851 (3353)	51246 (8196)	47155 (4695)	12743 (1885)	39239 (6208)	141779 (22195)
Rmerge (%)[a]	8.7 (72.2)	10.9 (66.9)	19.3 (92.4)	8.7 (92.7)	21.5 (91.8)	16.8 (92.1)	5.7 (121.0)
Completeness (%)[a]	100 (100)	99.5 (98.4)	99.2 (98.8)	99.9 (99.9)	96.8 (98.2)	99.5 (98.3)	98.7 (95.8)
Redundancy[a]	13.2 (13.7)	7.5 (7.3)	2.9 (2.9)	14.8 (15.4)	3.7 (3.8)	3.9 (3.9)	6.7 (5.9)
$\langle I \rangle / \langle \sigma I \rangle$[a]	18.4 (4.0)	14.6 (3.1)	7.9 (1.5)	23.9 (3.1)	2.9 (0.8)	10.1 (1.8)	20.0 (1.5)
Phasing/Refinement							
MR start model	4GV7	3KCZ	4GV7	4GV7	4L6S	4GV7	3HKV
Resolution (Å)	86.3 - 2.20 (2.26 - 2.20)	29.3 - 2.10	37.9 - 3.19 (3.32 - 3.19)	46.3 - 2.20 (2.26 - 2.20)	45.6 - 3.22 (3.53 - 3.22)	48.5 - 2.83 (2.98 - 2.83)	47.7 – 1.25 (1.28 – 1.25)
R_{work}/R_{free} (%)	20.30/21.79	18.98/23.10	19.17/26.87	24.99/27.98	23.76/27.29	19.49/24.51	20.81/21.26
No. of atoms							
Protein	10997	5609	10944	5550	5124	5556	3060
Ligand	96	64	48	56	44	42	36
Water	154	267	4	36	23	11	360
B-factors							
Protein	58.51	22.15	77.58	57.04	96.78	49.19	19.50
Ligand	34.25	17.39	71.86	60.72	71.82	54.90	14.62
Water	40.03	22.83	16.88	36.37	37.85	25.52	30.03
r.m.s. deviations							
bond lengths (Å)	0.010	0.017	0.010	0.019	0.008	0.010	0.011
bond angles (°)	1.1	1.5	1.2	2.0	1.0	1.2	0.9
Ramachandran plot							
Most favored (%)	98.4	97.6	95.9	96.3	94.7	97.1	98.4
Allowed (%)	100	98.0	100	99.8	99.7	100	100

[a] Numbers in parentheses denote the highest resolution shell.

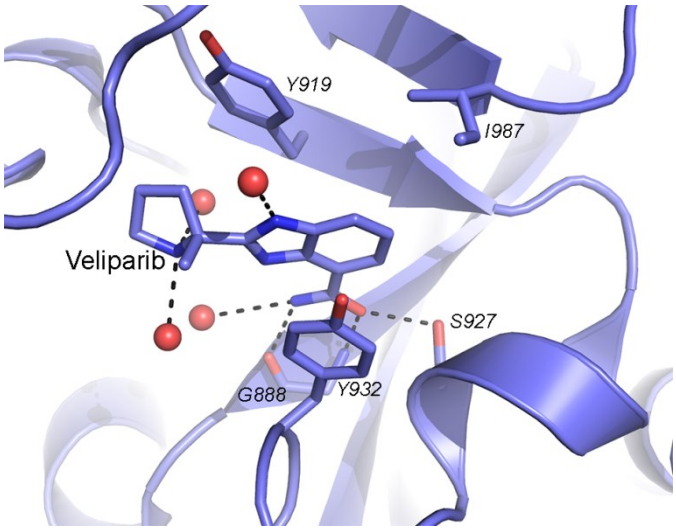

Figure S13. Active site of PARP10 with bound Veliparib. The ligand makes contact with protein side chains in the nicotinamide pocket, but no further direct interactions. Despite of this the ligand was well ordered, the D-loop was fully visible in the electron density, and the data allowed refining the model to 1.25 Å resolution. Protein Data Bank entry 5LX6.

Extended Materials and Methods

Recombinant protein production and purification – The cDNA fragments encoding the proteins listed in Table S1 were inserted into pNIC-Bsa4 or pNIC-CH2.[8] Protein expression in *Escherichia coli* strains BL21(DE3) pRARE or C41, and purification by immobilized metal affinity chromatography followed by size exclusion chromatography (SEC) were done as previously described.[9] Protein purity was 75-90 % as judged by SDS-PAGE followed by Coomassie staining. Integrity of all protein batches was verified by LC-ESI mass spectrometry. For control experiments displayed in **Figure S2**, human PARP1 protein was purchased from Sino Biological.

In vitro ADP-ribosylation assay – PARP automodification or histone modification was measured essentially as described before.[4] Briefly, 50-µl aliquots of hexahistidine-tagged PARP proteins (10 – 500 nM in 50 mM HEPES pH 7.5, 100 mM NaCl, 4 mM $MgCl_2$, 0.2 mM TCEP) were immobilized on Ni^{2+}-chelating plates (originally purchased from 5-PRIME, later ThermoFisher Scientific #15242). For PARP1, -2 and -3 proteins, sheared herring sperm DNA (Sigma-Aldrich) and recombinant hexahistidine-tagged histone H4 (PARP1) or H1 (PARP2, -3) were added. ADP-ribosyltransferase reactions were started by addition of 2% biotinylated NAD^+ (Trevigen) and incubated at 20°C. Reactions were stopped by addition of 100 µl (7 M) guanidine hydrochloride. Plate wells were washed with Tris-buffered saline containing 0.02% Tween-20 (TBST), incubated for 30 minutes with TBST containing 1% (w/v) BSA. After incubation with streptavidin-conjugated horseradish peroxidase (0.5 µg/ml; Jackson Immunoresearch) and washing, chemiluminescence detection was done using SuperSignal West Pico (ThermoFisher Scientific) in a CLARIOstar (BMG Labtech) microplate reader.

For concentration response experiments, NAD^+ concentrations were adjusted to K_M for each enzyme construct, or lower. IWR1 was kindly provided by Lawrence Lum (UT Southwestern Medical Center) and AZ-6102 was provided by AstraZeneca through the Open Innovation Program. All other PARP and tankyrase inhibitors were purchased from Selleckchem or Sigma-Aldrich. Compounds were added from stock solutions in DMSO followed by 15 min pre-incubation before addition of NAD^+. The final concentration of DMSO was 1% in all reactions. Compound stock solutions were stored at room temperature and DMSO from the same batch used for dilution was used in control reactions.

Table S4. Summary of PARP1 crystallization conditions and cryo-protectant solutions.

	Niraparib	**Rucaparib**	**Talazoparib**	**PJ34**	**XAV939**
Protein concentration	70 mg/ml	80 mg/ml	47 mg/ml	77 mg/ml	50 mg/ml
Precipitant	27% PEG-3350	27% PEG-3350	39% PEGMME-2000	25% PEG-3350	21% PEG-3350
Salt	0.2 M ammonium sulfate	0.2 M ammonium sulfate	0.2 M potassium thiocyanate	0.2 M ammonium sulfate	0.17 M ammonium sulfate
Buffer	0.1 M Bis-Tris	0.1 M Bis-Tris	0.1 M HEPES	0.1 M Bis-Tris	0.1 M Bis-Tris
pH	5.9	5.9	6.6	5.5	5.5
Inhibitor	1 mM Niraparib	1 mM Rucaparib	1 mM Talazoparib	20 mM PJ34	1 mM XAV939
Cryo-protectant	28% PEG3350, 0.2 M ammonium sulfate, 0.1 M Bis-Tris pH 5.8, 16% glycerol	28% PEG3350, 0.2 M ammonium sulfate, 0.1 M Bis-Tris pH 5.8, 16% glycerol	39% PEGMME-2000, 0.2 M potassium thiocyanate, 0.1 M HEPES pH 6.6, 10% glycerol, 1 mM Talazoparib	25% PEG3350, 0.2 M ammonium sulfate, 0.1 M Bis-Tris pH 5.5, 25% glycerol	22% PEG3350, 0.17 M ammonium sulfate, 0.1 M Bis-Tris pH 5.5, 20% glycerol, 0.2 M sodium chloride

Protein crystallization – All crystals were obtained by vapor diffusion in sitting drops at 4°C. Full conditions for obtaining PARP1 catalytic domain crystals are given in **Table S4**. Crystals of the PARP2 catalytic domain grew from a drop containing 0.1 µl protein (30 mg/ml including 10 mM 3-aminobenzamide) and 0.2 µl well solution (25% PEG-3350, 0.1 M Tris-HCl pH 8.5). After 6 weeks, rod-like crystals were soaked in well solution containing 5 mM Olaparib for 8 days, and stored under liquid nitrogen in cryo-solution (26% PEG-3350, 0.1 M Tris-HCl pH 9.0, 0.2 M NaCl, 15% glycerol, 2 mM Olaparib). Crystals of the PARP10 catalytic domain (N819-V1007) grew from a drop containing 0.2 µl protein (10.5 mg/ml including 2 mM Veliparib) and 0.1 µl well solution (12% PEG-3350, 0.1 M ammonium tartrate pH 7.0). Large (30 x 300 µm) crystals appeared after 3 weeks. Crystals were stored under liquid nitrogen in cryo-solution (13% PEG-3350, 0.1 M ammonium tartrate pH 7.0, 0.2 M NaCl, 28% glycerol).

Structure determination and refinement – Diffraction data (**Table S3**) were indexed, integrated using XDS,[10] scaled and truncated using SCALA or XSCALE and the CCP4 suite of programs.[11] BESSY synchrotron diffraction data were processed using XDSAPP.[12] The structures were solved by molecular replacement with PHASER.[13] All structures were refined using Refmac5[14] or Buster,[15] and model building was done with Coot.[16]

References

1. Karlberg, T.; Klepsch, M.; Thorsell, A. G.; Andersson, C. D.; Linusson, A.; Schüler, H. Structural basis for lack of ADP-ribosyltransferase activity in poly(ADP-ribose) polymerase-13/zinc finger antiviral protein. *The Journal of biological chemistry* **2015,** *290* (12), 7336-7344.
2. Vyas, S.; Chesarone-Cataldo, M.; Todorova, T.; Huang, Y. H.; Chang, P. A systematic analysis of the PARP protein family identifies new functions critical for cell physiology. *Nat. Commun.* **2013,** *4*, 2240.
3. Langelier, M. F.; Planck, J. L.; Roy, S.; Pascal, J. M. Structural basis for DNA damage-dependent poly(ADP-ribosyl)ation by human PARP-1. *Science* **2012,** *336* (6082), 728-732.
4. Langelier, M. F.; Planck, J. L.; Servent, K. M.; Pascal, J. M. Purification of human PARP-1 and PARP-1 domains from Escherichia coli for structural and biochemical analysis. *Meth. Mol. Biol.* **2011,** *780*, 209-226.
5. Langelier, M. F.; Ruhl, D. D.; Planck, J. L.; Kraus, W. L.; Pascal, J. M. The Zn3 domain of human poly(ADP-ribose) polymerase-1 (PARP-1) functions in both DNA-dependent poly(ADP-ribose) synthesis activity and chromatin compaction. *J. Biol. Chem.* **2010,** *285* (24), 18877-18887.
6. Langelier, M. F.; Servent, K. M.; Rogers, E. E.; Pascal, J. M. A third zinc-binding domain of human poly(ADP-ribose) polymerase-1 coordinates DNA-dependent enzyme activation. *J. Biol. Chem.* **2008,** *283* (7), 4105-4114.
7. Ali, A. A.; Timinszky, G.; Arribas-Bosacoma, R.; Kozlowski, M.; Hassa, P. O.; Hassler, M.; Ladurner, A. G.; Pearl, L. H.; Oliver, A. W. The zinc-finger domains of PARP1 cooperate to recognize DNA strand breaks. *Nat. Struct. Mol. Biol.* **2012,** *19* (7), 685-692.
8. Strain-Damerell, C.; Mahajan, P.; Gileadi, O.; Burgess-Brown, N. A. Medium-throughput production of recombinant human proteins: ligation-independent cloning. *Meth. Mol. Biol.* **2014,** *1091*, 55-72.
9. Wahlberg, E.; Karlberg, T.; Kouznetsova, E.; Markova, N.; Macchiarulo, A.; Thorsell, A. G.; Pol, E.; Frostell, A.; Ekblad, T.; Oncu, D.; Kull, B.; Robertson, G. M.; Pellicciari, R.; Schuler, H.; Weigelt, J. Family-wide chemical profiling and structural analysis of PARP and tankyrase inhibitors. *Nat. Biotechnol.* **2012,** *30* (3), 283-288.
10. Kabsch, W. XDS. *Acta Cryst. D Biol. Crystallogr.* **2010,** *66* (Pt 2), 125-132.
11. Evans, P. Scaling and assessment of data quality. *Acta Cryst. D Biol. Crystallogr.* **2006,** *62* (Pt 1), 72-82.
12. Goenka, S.; Boothby, M. Selective potentiation of Stat-dependent gene expression by collaborator of Stat6 (CoaSt6), a transcriptional cofactor. *Proc. Natl. Acad. Sci. U.S.A.* **2006,** *103* (11), 4210-4215.
13. McCoy, A. J.; Grosse-Kunstleve, R. W.; Storoni, L. C.; Read, R. J. Likelihood-enhanced fast translation functions. *Acta Cryst. D Biol. Crystallogr.* **2005,** *61* (Pt 4), 458-464.
14. Murshudov, G. N.; Skubak, P.; Lebedev, A. A.; Pannu, N. S.; Steiner, R. A.; Nicholls, R. A.; Winn, M. D.; Long, F.; Vagin, A. A. REFMAC5 for the refinement of macromolecular crystal structures. *Acta Cryst. D Biol. Crystallogr.* **2011,** *67* (Pt 4), 355-367.
15. Johannes, J. W.; Almeida, L.; Barlaam, B.; Boriack-Sjodin, P. A.; Casella, R.; Croft, R. A.; Dishington, A. P.; Gingipalli, L.; Gu, C.; Hawkins, J. L.; Holmes, J. L.; Howard, T.; Huang, J.; Ioannidis, S.; Kazmirski, S.; Lamb, M. L.; McGuire, T. M.; Moore, J. E.; Ogg, D.; Patel, A.; Pike, K. G.; Pontz, T.; Robb, G. R.; Su, N.; Wang, H.; Wu, X.; Zhang, H. J.; Zhang, Y.; Zheng, X.; Wang, T. Pyrimidinone nicotinamide mimetics as selective tankyrase and wnt pathway inhibitors suitable for in vivo pharmacology. *ACS Med. Chem. Lett.* **2015,** *6* (3), 254-259.
16. Emsley, P.; Lohkamp, B.; Scott, W. G.; Cowtan, K. Features and development of Coot. *Acta Cryst. D Biol. Crystallogr.* **2010,** *66* (Pt 4), 486-501.